Nano-structured materials for the electrochemiluminescence signal enhancement

(Article begins on next page)

28 April 2024

Nano-structured materials for the electrochemiluminescence signal enhancement

Pavlos Nikolaou, Giovanni Valenti, Francesco Paolucci*

Department of Chemistry "G. Ciamician" University of Bologna, Via Selmi 2, 40126, Bologna (Italy)
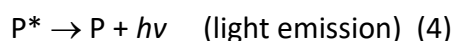E-mail: francesco.paolucci@unibo.it

Abstract: Electrochemiluminescence (ECL) is an electrochemically induced emission where the nature of electrode materials strongly affects the kinetics of the heterogeneous electron transfer with an impact on the final ECL performance. Different types of electrodes have been tested in view of their nanoscale properties. In this review we summarize the ECL behavior of various types of nano-structured electrodes highlighting the capability to enhance the ECL signal using different coreactants. Signal generation strategies and analysis of the applications are discussed in detail with particular attention to the challenges and future prospects in the field of ECL.

Keywords: Electrochemiluminescence, electrochemistry, nanomaterials, ECL enhancement, modified electrodes.

1. Introduction

Electrochemiluminescence, or electrogenerated chemiluminescence (ECL), is a controllable form of chemiluminescence (CL) initiated and produced from an electron-transfer reaction taking place on the surface of the electrode and yielding light-emitting excited states [1–6]. As far as it is known, the first ECL phenomenon was presented in 1927 by Dufford et al. from the observation of light emission during the electrolysis of Grignard compound in anhydrous media [7]. Generally, the principal mechanism of ECL is generated via annihilation, which involves homogeneous electron transfer reactions between electrochemically generated anions and cations which are produced on the surface of the electrode [8]. This annihilation mechanism is presented below [Eq. 1-4]:

$$P \rightarrow D^+ + e^- \quad \text{(oxidation at electrode)} \quad (1)$$

$$P + e^- \rightarrow A^- \quad \text{(reduction at electrode)} \quad (2)$$

$$D^+ + A^- \rightarrow P^* + P \quad \text{(excited state formation)} \quad (3)$$

$$P^* \rightarrow P + h\nu \quad \text{(light emission)} \quad (4)$$

in which P = luminophore, D+ = oxidized luminophore, A- = reduced luminophore and P* = luminophore excited state.

The luminophores A^- and D^+ are usually highly reactive or unstable species, so their generation and the annihilation reaction must be carried out in pure and aprotic solvents with large potential windows [9][10].
However, in the 1980's Bard and co-workers [5] proposed a different approach to the generation of ECL in protic media, and in particular water, whose mechanism was based on the reaction between a so-called coreactant and the luminophore. This strategy opened the

application of ECL to aqueous environments, thus making it suitable for the analysis of bio-related samples. Typically, in coreactant-ECL, the excited state is generated through the reaction between two different precursors, an emitter (i.e., the luminophore) and a coreactant chosen among various classes of chemicals, whose fundamental feature is to present a highly unstable oxidized (or reduced) form that undergoes a fast-chemical degradation, thus forming a high-energy radical. Two different mechanisms are then possible, depending on the nature of the coreactant, namely, the oxidative-reduction or the reductive-oxidation one. In all cases, the rate-determining steps for the overall process include, the kinetics underlying the heterogeneous electron transfer reactions of the coreactant, the stability of coreactant radicals, and the distribution of ECL luminophores can influence the ECL efficiency [11][12].

The most used systems for coreactant ECL is the combination in aqueous media of *tripropyl-n-amine* (TPrA) as coreactant and tris(2,2'-bipyridine) ruthenium (II) [Ru(bpy)$_3^{2+}$] as emitter.

[Please insert here Figure 1]

In such a system, the application of a positive enough potential drives the simultaneous oxidation of both Ru(bpy)$_3^{2+}$ and TPrA, that are both free to diffuse in solution (Fig.1a). By contrast, in the commercial immunoassay application, the luminophore Ru(bpy)$_3^{2+}$ is usually anchored, following the biorecognition event, onto, e.g., the surface of a magnetic microbead at such a distance from the electrode surface that prevents any direct electron transfer to the electrode. Bard and co-workers proposed a variant of the previous mechanism explaining the observation of the ECL emission under such conditions, i.e., when oxidation of TPrA can only occur[13]. Such a mechanism involves both TPrA$^{\bullet}$ and TPrA$^{\bullet+}$ (Fig. 1b). Amatore and co-workers analyzed this mechanism using digital simulation to investigate the kinetic and thermodynamic parameters associated with the ECL generation [14]. They also examined the effect of the diffusion coefficient, of both coreactant and ECL-active luminophore, on the ECL mechanism and found that the relative contribution of the ECL mechanisms changes from Fig. 1(a) to Fig. 1(b) by decreasing the diffusion coefficient of the luminophore. More recently, further insights in the latter mechanism, also named "remote ECL", were obtained by us through the analysis of size-effects in microbead-based ECL [15].

An important factor determining the efficiency of the ECL generation is the nature and chemical and physical state of the electrode surface where the ECL process is initiated. In fact, one of the key steps for the optimization of the signal-to-noise ratio is the heterogeneous electron transfer reaction involving the coreactant whose kinetics may largely differ for different electrode materials. Furthermore, it is well known that the electrode surface may be modified during the potential step (or scan) used in the ECL generation and this may dramatically affect the efficiency of the emission intensity. In fact, the electrode surface property might also affect the deprotonation reaction kinetics and therefore the lifetime of TPrA$^{\bullet+}$, thus influencing the spatial distribution of the radicals TPrA$^{\bullet}$ in the diffusion layer also determining the extent of the scavenging oxidative reaction indicated by the dashed line in Fig. 1(b). Moreover, the adsorption of intermediates, such as radical cation or coreactant by-products, is known to poison the electrode surface and decrease the ECL intensity upon prolonged and/or repeated emission.

Many nanomaterials have demonstrated their useful application in the biosensors' field. The use of nanomaterials to immobilize biomolecules led in several examples to enhanced performance in terms of lower detection limits [16] often associated to very high stability and reproducibility [17]. The avidin-biotin complex is another system which can make some nanomaterials (gold nanoparticles, gold-silver nanoparticles, QDs and CNTs) suitable for their use in biosensor applications[18]. Some specific properties such as size, structure and target-specific binding [19] could be used for the enhancement of electrochemical signal of quantum dots [20] and for the immobilization of biomolecules in organic systems [21].

[Please insert here Figure 2]

In addition, one of the key parameters in the construction of a biosensor is the immobilization of a receptor onto the transducer unit. Nanomaterials (some examples are reported in Fig. 2 and described in detail below) are largely used for the immobilization of biomolecules both via physical adsorption or chemical anchoring. In fact the proper orientation of the receptor bio- molecules is critical because it must retain its bioactivity, while providing accessibility to the target analyte and a direct interaction with the transducer surface[22–25].

In such systems, the electron transport can occur by hopping between redox molecules, or through the conduction band of the nanomaterial matrix. The latter only occurs when the nano-based electrodes are rendered sufficiently conducting by applying the necessary potential and is a random-walk diffusion process, as in novel applications of ECL resonance energy transfer and ECL imaging [26–28]. Important advantages are often associated to the specific characteristics of their surface. Nanoporous based materials often present a surface area typically much larger than the geometric area. This large surface area, in view of their pores of similar dimensions, is capable to host biomolecules for the investigation of bio-electrochemical sensors [29]. Herein, this surface could combine advantages of single-molecule sensing and high selectivity for biomolecules such as DNA [30]. The properties of nanoporous alloys are not only useful in bio-applications but also in electrocatalytic systems possibly bringing to enhanced durability [31]. Nanoporous alloys materials were used for the immunological determination of proteins and antigens [32].
Additionally, we recently presented the effect of combined homo- and heterogenous charge transfer in nanosystem-based ECL where the ECL intensity was largely affected by the size and surface properties of nanomaterials [33][34]. In this context the control of the surface propriety, charge of the nanomaterial and structure have been applied as novel strategies for enhance the ECL analytical signal.

This review analyzes the various nanostructured materials and their effect on ECL generation focusing of the modification of electrodes as a pathway for the enhancement of the analytical signal. This category of materials will not only be limited to the $Ru(bpy)_3^{2+}$/TPrA system, but we will also analyze other coreactants and systems such as H_2O_2, $K_2S_2O_8$ and $(NH_4)_2S_2O_8$.

2. Nano-structured materials
2.1 Nanoparticles

Various nanoparticle materials such as palladium [35], platinum [36] and gold [37] are typically used in electroanalysis, due to their good conductivity, high surface area and high chemical stability. They can easily be used to modify the surface of other such as carbon-based substrates endowing them with enhanced properties. Silver nanoparticles (AgNPs) display excellent antibacterial, electrical, optical, catalytic and surface-enhanced Raman properties [38]. Also, commercial electrodes, such as stainless steel electrode (type 304) have been used for the enhancement of ECL signals with the luminol/H_2O_2 system [39].

Nanocrystals (NCs) are also typically found among the nanoscale materials. NCs have been investigated also for biosensing applications in ECL systems as aggregation-induced enhanced electrochemiluminescence emitters [40], as emitters for immunosensing [41] and coreaction accelerators [42]. Fig.3 presents a procedure for the development of an ultrasensitive sandwich ECL biosensor. The design is based on using the Ag^+@UIO-66-NH_2 enriched CdWS (NCs) as a multifunctional signal probe for the quantitative evaluation of the prostate cancer marker (PSA). Beside nanoparticles, the combination of metals-non metals or metals-quasi metals as CdTe and CdSe leads to the creation of nanocrystals. Many works were focused on the synthesis of dual-stabilizer-capped NCs, which Zou et al. reported to exhibit excellent ECL behavior [43]. The dual-stabilizer-capped NCs not only effectively remove the non-radiative surface states and deep surface traps, but also accelerate electron and hole injection in the cathodic ECL process, giving rise to increased ECL efficiency [43]. Also, the dual potential ECL can open new way for further investigation in this field using NCs [44].

[Please insert here Figure 3]

The development of new modified electrodes opened new horizons for the enhancement of ECL intensity, among which, the nanoneedle array electrodes attracted a large interest because of the strong increase of the ECL signal associated to enhanced mass transfer [39].

It is worth noticing in such a context that an increase of the ECL signal is not necessarily associated to the preparation of bulk nanomaterials. Surface chemical treatment can also effectively affect the performance. Qiao et al. [37] reported that 1,6-hexanedithiol can be absorbed on the gold electrode surface during a hydrophobic reaction eventually leading to a three-fold ECL improvement with the luminol system (Fig.4). Alkanethiolates have long been used for the creation of self-assembled monolayers (SAMs) onto gold electrodes. These films have widely been studied for biosensing applications for their electrochemical, electrocatalytic, redox properties and biocompatibility [45–52]. Although some research groups have reported the combination of luminol ECL sensing methods with the SAMs modified electrodes, these works mainly focused on the immobilization of DNA probes or nanomaterials on gold electrodes [53–55].

[Please insert here Figure 4]

Within the large range of electrochemical applications, Au electrodes were mostly tested in aqueous solutions [56–58]. Au electrodes have been used with the TPrA/Ru(bpy)$_3^{2+}$ system in which it presents ECL efficiency 10 times larger than on Pt under similar conditions [59][56]. An important factor in ECL technology, strongly determining its versatility, is electrode transparency [60]. In some cases, gold nanoparticles (AuNPs) were chosen to modify transparent electrodes such as FTO because of their unique electrochemical, catalytic and chemical properties. Transparent AuNPs-FTO electrodes were fabricated by electrodeposition of AuNPs onto the surface of the FTO electrode. Such electrodes are capable to detect H$_2$O$_2$ released from living cells via the luminol-H$_2$O$_2$ ECL transduction approach. These electrodes keep the limit of detection (LOD) at very low levels (8nM), as Li et al reported, and are at the same time characterized by great stability and selectivity and are suitable for the investigation of several biological systems [61].

Beside AuNPs, also other metal-nanoparticles have shown great properties in the context of ECL biosensing. Platinum nanoparticles (PtNPs) and, specifically, the nanoflowers (PtNFs) were used in combination with rubrene microrods (RubMRs). The Pt nanostructure can be used as co-reaction accelerator which leads to a novel approach for the detection of biomolecules. To describe a possible ECL mechanism the in-situ grown PtNFs@RubMRs deposited onto GC electrodes were investigated in H$_2$O$_2$/PBS solutions between -1 to 1.2 V and in either the presence or in the absence of oxygen (Fig.5c). Firstly, only the luminophores group (RubMRs) was investigated (Fig.5 a-b). The ECL signal in the presence of O$_2$ was about 43 times higher than that in N$_2$-saturated PBS, showing the participation of the reactive oxygen species (ROS) in the creation of the excited state (Rub*) [62]. After the modification with PtNFs, the ECL signal was 14 times stronger than that on the bare RubMRs [36].

[Please insert here Figure 5]

Nanocrystals (NCs) also found wide applications for the development of novel ECL-based biosensing systems. They have typically a narrow band gap and may be effectively associated with a metal-oxide surface into which electrons, coming from the NC conduction band, are easily injected. An example is CdS NCs deposited on TiO$_2$ nanotube (NT) films reported by Dai et al. [63]. The electronic coupling with the semiconductor nanomaterials facilitates holes transfer from the VB of TiO$_2$ to CdS finally resulting in the generation of excited CdS* and enhanced ECL. Within this doping model, three different electrodes, i.e., bare TiO$_2$ NTs, CdS/TiO$_2$ NTs, either as is or after activation by immersion in a H$_2$O$_2$ and sodium citrate solution were compared. After the activation, the value of ECL intensity was 3.77 and 265 times stronger than the as is or bare ones, respectively. The cyclic voltammetry analysis showed a significant increase of H$_2$O$_2$ reduction current on the activated electrode. The effect was sensitive to the number of CdS layers deposited onto the TiO$_2$ surface: the ECL response greatly increased up to three monolayers while thicker films inhibited the directional charge transport within the tubes, resulting in decreased ECL emission.

2.2 Carbon based hybrid materials

Nanocarbon-based materials have played an important role in the field of ECL. The high conductivity and stability at positive potentials allows the oxidation of the coreactant and also affects the deprotonation reaction kinetics and therefore the lifetime of TPrA$^{\bullet+}$, thus influencing the spatial distribution of the radicals [64]. Carbon-based materials can be combined with other materials as described in section *2.1.*[65] [66], for the creation of specific modified electrodes which have found wide use in electrochemistry in general, and also combines transparency with a high electroactive surface area [66]. In particular, carbon nanotubes (CNTs) with their high specific surface area, chemical stability and super electrocatalytic properties are worldwide used electrodes in ECL biological systems and spectroelectrochemical devices [64,67–71].

Commercial electrodes as glassy carbon electrode (GCE) can be modified by CNTs as well. The properties of GCE electrodes such as high chemical stability and high conductivity [72] [73] can be modified with the immobilization of nanomaterials. Also, it has been demonstrated their extreme resistance under electrochemical oxidative conditions, which occur under oxygen-involving reactions like oxygen reduction reaction and oxygen evolution reaction [74]. GCE exhibits excellent stability when it is used in acid and basic solutions. Biocompatibility and stability are some of the properties of GCE which made it suitable in the field of electrochemical biosensing [75][76]. Following surface pretreatment (laser activation, electrochemical oxidation, and heating) the fresh carbon sites are exposed and oxygen containing groups are produced on the surface of electrode. Such surface groups can then host specific ruthenium luminophores and, as a result, this system may be used in ECL [77][78].

The electrode surface of a GCE electrode typically displays a very limited porosity. Graphene, on the other hand, forms aggregates on the electrodes surface and exhibits planar stacking structures due to the strong π-interaction between the graphene sheets, which results in the decrement of the specific surface area and blocking of the mass transfer [79][80]. The use of three-dimensional porous graphene deposited on GCE may exhibit unique properties as large specific surface area, porous structure and high mass transfer [81]. These type of electrodes (graphene-chitosan and three-dimension porous graphene) were investigated as biosensors by immobilization of glucose oxidase [82], thus the properties as compared to a bare graphene electrode were improved. Xu et al.[83] reported three different types of GCE which were used for the ECL signal enhancement. This category of materials can be chemically treated to host specific molecules, such as the luminophore [Ru(bpy)$_2$phendiamine]$^{2+}$ (Ru-L1). The link between the oxidised GCE surface (GCEox) and Ru-L1 is achieved when the GCEox exhibits a negatively charged surface tending to attract and react with the amino group of Ru-L1. The bonding gives Ru-GCEox hybrid an excellent solid ECL electrode performance. Ru-GCEox shows reusability after long-term storage, with a slight polishing treatment, which makes it a reliable ECL sensor.

Firstly, a bare GCE, a GCEox and a Ru-GCEox were investigated in PBS solution. As shown in Fig. 6 (a) Ru-GCEox displays an additional oxidation peak (0.7V) compared with the CVs of bare GCE and GCEox. This peak has appeared because of the immobilization of Ru species on the

GCE surface. Furthermore the electrochemical behavior of these electrodes was investigated in $Fe(CN)_6]^{3+/4+}$ solution, the peak potential differences of bare GCE, GCEox and Ru-GCEox increasing from 90 mV to 200mV, indicative of increasing irreversibility in line with an increasing surface resistance from bare GC to GCEox and Ru-GCEox (Fig. 6 (b)). However, Ru-GCEox exhibits an obvious higher ECL signal as it is presented in Fig. 6(c), (d) both in the absence and in presence of TPrA, an important coreactant to create excited states for ECL process. This result indicates the successful bonding of Ru-L1 on Ru-GCE surface and the capability of the electrode to enhance the ECL signal using chemical treatment. An important factor is the thickness of the immobilized specific compound on the surface of GCEox. According to the diffuse double layer theory, the charges would be assembled on the GCE surface in the process of electron conditioning. The charge with the opposite polarity in the background electrolyte will be attracted on GCE surface and form an electric double layer. The distance of the change between the Ru-L1 and GCEox could give us the distance, which is approximately some nanometers [84]. This chemical treatment, if Ru-L1 incorporated in Nafion film coated in GCE, the charge transfer distance between Ru-L1 and GCE surface is increased to include the phase interface gap and the thickness of the film, something which will be probably worked as an effect of the ECL signal. Finally, the lower ECL potential of Ru-GCEox indicated the higher charge transfer rate between Ru-L1 and GCE surface.

[Please insert here Figure 6]

On the other hand, the immobilization of biomolecules on the surface of carbon-based electrodes such as GCE is difficult without pretreatment. A possible way for the creation of a carbon-based electrode with high porosity is the combination with metal oxides (MOx). Many works present the MOx as materials with high surface area, large band-gap value, optically transparent, electrochemically stable and several are used as a layer for the immobilization of biomolecules or organic/inorganic molecules for the development of chemical sensors [85–88]. The most known and used MOx material in ECL system is titanium dioxide (TiO_2) as it presents high conductivity at negative potentials and can be easily doped with other conductive materials. There are three crystalline forms of TiO_2: anatase, rutile and brookite. The uses of TiO_2 nanomorphologies as nanosheets [89], nanopillars [90], nanoarrays [91] , nanoparticles [92], nanorods [93], nanowires [94] , nanoneedles [95] [96] , nanoflowers [97] , nanocubes [98] and mesocrystals [99] [100] have been reported for bioanalytical uses. Topoglidis et al.[101] presented TiO_2 nanoporous structure for the enhancing of active surface area of a conductive glass and for immobilization and biosensing uses. TiO_2 has a surface area which is typically much greater (by up to 1000 times) than its geometric area. The porous size diameter is about 10-20 nm that is an ideal porosity for protein immobilization. In this case the proteins remain immobilized in the surface of the film. The protein is furthermore stabilized and constrained by the pores of the film.
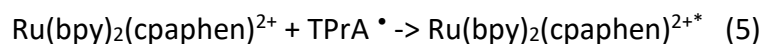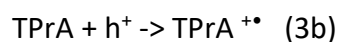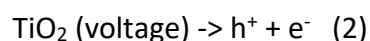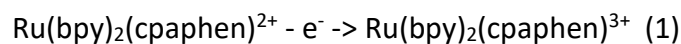
TiO_2 nanoneedles (NNs) was synthesized and was deposited onto GCE electrode surface with the help of multi-wall carbon nanotubes (MWCNTs); in this way, a commercial electrode can
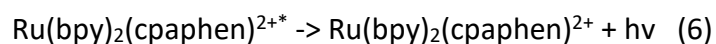
be combined with these types of materials. Zhang et al [96] reported the case of GCE/MWCNTs/TiO$_2$ NNs which promote an enhancement in ECL intensity. The ECL measurements were made to explore the possible reaction mechanism. As shown in Fig.7A, the ECL signal of TiO$_2$ NNs modified GCE (curve b) and bare GCE (curve a) did not present a significant difference without TPrA as coreactant. On the other hand, when TPrA was added, it creates excited states and the luminophore, in this case bis(2,2'-bipyridy) (5-amino-1,10-phenanthroline) ruthenium (II) (Ru(bpy)$_2$(cpaphen)$^{2+}$), can generate high ECL intensity because the deprotonation of TPrA is accelerated by the TiO$_2$ NNs. Inspired by this mechanism, the hybrid electrode GCE/MWCNTs/TiO$_2$NNs was used as accelerator in ternary system for the deprotonation of TPrA [102–104][96]. The CV characterization is presented in Fig.7B with the cyclic potential scanning from 0 to 1.25V. The peak current of TiO$_2$ NNs modified GCE (curve b) and bare GCE (curve a) show similar morphology in Ru(bpy)$_2$(cpaphen)$^{2+}$ solution. In the presence of TPrA, bare GCE displays significantly higher anodic currents (curve d), associated to the generation of large amounts of oxidized TPrA species at the electrode surface and a much larger increase of current (and TPrA production rates) are observed in the case of TiO$_2$ NNs modified GCE (curve e). Finally, current further increased when both TPrA and Ru(bpy)$_2$(cpaphen)$^{2+}$) were present (curve f), as expected for the activation of the catalytic mechanism enhanced by TiO$_2$ NNs playing the role of coreaction accelerator of the TPrA oxidation rate.

Finally, Fig.7C shows the maximum ECL emission wavelength of Ru(bpy)$_2$(cpaphen)$^{2+}$)/TPrA solution at 625 nm, as reported by Zhang et al [96]. When the TiO$_2$ NNs were coated onto GCE, the ECL response of Ru(bpy)$_2$(cpaphen)$^{2+}$)/TPrA solution increased and the maximum emission wavelength was shifted (Fig. 7D), thus showing an interaction of the luminophores with the surface.

A possible mechanism of the observed enhancing effect comprises the generation, upon the application of the voltage, of electron-holes couples in TiO$_2$ (Eq 2) [97][105]. Holes would then migrate to the surface and would be involved, along with the usual anodic oxidation, in the promotion of TPrA$^{+\bullet}$ generation, then resulting in more TPrA$^{\bullet}$ (through the deprotonation process) and eventually in brighter ECL signal [96].

[Please insert here figure 7]

$$Ru(bpy)_2(cpaphen)^{2+} - e^- \rightarrow Ru(bpy)_2(cpaphen)^{3+} \quad (1)$$

$$TiO_2 \text{ (voltage)} \rightarrow h^+ + e^- \quad (2)$$

$$TPrA - e^- \rightarrow TPrA^{+\bullet} \quad (3a)$$

$$TPrA + h^+ \rightarrow TPrA^{+\bullet} \quad (3b)$$

$$TPrA^{+\bullet} \rightarrow TPrA^{\bullet} + H^+ \quad (4)$$

$$Ru(bpy)_2(cpaphen)^{2+} + TPrA^{\bullet} \rightarrow Ru(bpy)_2(cpaphen)^{2+*} \quad (5)$$

$$Ru(bpy)_2(cpaphen)^{2+*} \rightarrow Ru(bpy)_2(cpaphen)^{2+} + hv \quad (6)$$

The combination of MOx (TiO_2) and carbon-based materials for ECL generation was reported by Han et al [106] who used nanographene oxide which is capable to wrap the titanium dioxide nanoparticles (nGO@TiO_2 NLPs). This system was investigated using $K_2S_2O_8$ as a coreactant. The ECL property of this system together with its cyclic voltammetry response is presented in Fig.8.

[Please insert here Figure 8]

Noteworthy, this system shows the presence of two ECL peaks (ECL-1 and ECL-2), both occurring during the scan in the negative potential region. As shown in Fig. 8(a) both TiO_2 and nGO have only one ECL peak in the same conditions. These assignments of ECL-1 and ECL-2 were further explored by the ECL spectra of nGO@TiO_2 NLPs. The maximum ECL emission wavelengths of ECL-1 and ECL-2 were observed at 510 and 535 nm (Fig. 8(c), (d)) respectively, which were consistent with that of TiO_2 and nGO. All the above results demonstrate that ECL-1 and ECL-2 derived from the combination of these two nanomaterials. This system has been tested also in air-saturated conditions evidencing an enhancing effect of O_2. It was reported that O_2 could be reduced to peroxide anion at a negative potential corresponding to ECL-1 [107] while ECL-2 resulted from the reaction between nGO and $S_2O_8^{2-}$. For ECL-1, O_2 was first reduced to OOH^-, which could react with $S_2O_8^{2-}$ to generate $SO_4^{\bullet-}$ [107]. When $S_2O_8^{2-}$ was partially consumed during the ECL-1 process of nGO@TiO_2 NLPs, the ECL-2 signal decreased. On the other hand, $S_2O_8^{2-}$ could also be directly electroreduced to $SO_4^{\bullet-}$ (Fig. 8 (b)). Finally, a hole (h^+) generated by $SO_4^{\bullet-}$ was injected into the valence band of TiO_2, which could recombine with electrons from the conduction band of TiO_2, accompanying the light emission. For the ECL-2 process, $nGO^{\bullet-}$ electroreduced from nGO could react with $SO_4^{\bullet-}$ to form the excited state product nGO^* with light emission [108].

In conclusion, the reported electrodes have excellent electrochemical properties, enhanced ECL emission and great biocompatibility associated to the nature of TiO_2. Both can be used in positive and negative potential with different coreactants [106][96].

2.3. Nanocomposite materials

One of the main problems in electrochemistry is the conductivity and the stability of the materials which are used as electrode substrates. This is an important factor in ECL where the applied potential is typically quite high. Nanocomposite materials can combine the conductivity with the properties of the electroactive molecular, clusters or extended inorganic species allowing the design of novel materials with enhanced stability, charge propagation dynamics [109] and ECL activity [110].
Yan and co-workers [111] focused on the preparation of Pt and Au nanocomposites increasing the ECL signal of a biosensor, based on the luminol/H_2O_2 system, for kinase activity analysis

and inhibitor screening. According to the great catalytic activity of the Au/Pt nanoparticles, the ECL signal was largely improved, because of the acceleration of the H_2O_2 decomposition to produce $OH^\bullet$ and $O_2^{\bullet-}$ species, and, at the same time, for the acceleration of luminol oxidation [112][113]. It was clear that the ECL signal from the Au/Pt was much higher than the single Pt and single Au. This combination indicates the enhanced catalysis ability of Au and Pt bimetallic nanoparticles loaded in metal-organic frameworks (MOFs) for the creation of nanocomposites. MOFs have some benefits such as well-ordered porosity, high specific surface area and chemical tunability [114]. In ECL systems, MOFs have also been used for the development of biosensors with enhanced signal intensity. Owing to the large specific area, this wide category of materials allows to increment the amount of immobilized luminophores which, combined with the stable structure of MOFs, enhances the sensitivity and stability of ECL devices [115].

[Please insert here Figure 9]

As shown in Fig. 9, the ECL signal from the Au/Pt nanoparticle-loaded probes is compared with those obtained with either Pt or Au. The bimetallic nanoparticles were loaded in the probes to act in the catalytic mechanism and increase the signal, as it is observed in Fig. 9(c), which results much more intense than the simple addition of signals from either Pt or Au. This combination also confers good stability, when the ECL signal had not changed over 20 cycles.

Another type of modification with the use of Pt has been studied by Zhou et al [110]. The tri-metallic combination of Pt, Au and Ag which is used for the first time as an accelerator to significantly enhance ECL signal from a hollow porous graphitic carbon nitride (HP-C_3N_4) electrode using $S_2O_8^{2-}$ co-reactant. The HP-C_3N_4 is used as a platform to host the tri-metallic combination as the main application in the sensing of insulin using DNA walker amplification. Graphic carbon nitride (g-C_3N_4) electrodes were studied and investigated as a metal free composition, nontoxic material, and good biocompatibility [116–118]. The HP-C_3N_4 electrodes verify the novelty as a luminophore with excellent ECL efficiency which was expected to achieve a strong ECL signal. The use of single Pt materials as Pt nanoflowers and the Pt-Ag alloy were analyzed above in this review. Herein, in this point the nature and conductivity of tri-metallic AuPtAg accelerator was investigated in ECL system and show a self-accelerated ECL-biosensing platform.

[Please insert here Figure 10]

As it has been shown in Fig.10, the ECL signal is increased according to the material that is used on the surface of the principal electrode. The tri-metallic materials used as a coreaction accelerator can enormously enhance the ECL intensity by its catalytic property for $S_2O_8^{-2}$ reduction. The AuPtAg@HP-C_3N_4 electrode displays 14 times higher signal than the bare HP-C_3N_4 electrode.

2.4 Commercially available electrodes with nanoporous properties

Almost every commercially available electrode, such as Au electrodes, is characterized by scarce porosity and the modification of such electrodes can strongly influence the ECL signal. Many works have been reported based on the use of nanoporous Au electrodes and, in the case of ECL, the thickness and the pores size in nanoporous Au electrodes (NPG) have shown to be important factors for signal enhancement [119]. NPGs are typically obtained by chemical and electrochemical selective dissolution of Ag from Ag-Au alloys [120–122]. The sensing applications of this type of modified electrodes have been reported by several groups [123][124]. Villani et al [125] focused on NPG electrodes displaying different thickness and roughness specifications. As it is presented in Fig. 11, using a chronoamperometric technique, in the presence of chromophore and coreactant (0.01 mM [Ru(bpy)$_3$]Cl$_2$ and 30 mM TPrA respectively) an intense ECL emission is measured. The figure compares three different types of electrodes, a flat Au electrode, an NPG 120 nm (pore size) electrode and an NPG 200 nm (pore size) electrode. Although, the ECL signal is dependent on the surface geometry (flat vs. porous) and the ECL signal was found in all cases to decay with time, a behavior that has been associated with combined mass transport and surface passivation effects [50]. In addition, has been shown that the ECL intensity is reduced after the first scan in positive potential. This result comes from the degradation of electrocatalytic properties of the electrodes which is not capable to maintain the same value of ECL intensity.

[Please insert here Figure 11]

However, it has been shown that the ECL intensity is reduced after the first scan in positive potential. This result comes from the degradation of electrocatalytic properties of the electrodes which is not capable to sustain a fast coreactant reduction rate. As a matter of fact, surface analysis (by AFM) of electrodes in either pristine state and following the potential step highlighted a significant increase by 2-3 times of pore sizes after the ECL experiment. Such a remarkable surface modification was considered responsible for the irreversible degradation of NPG electrodes performance through a destabilization of the nanoporous structure and its partial dissolution making the NPG unsuitable for ECL generation using the [Ru(bpy)$_3$]$^{2+}$/TPrA system.

Efficient ECL generation with NPGs was instead obtained with (NH$_4$)$_2$S$_2$O$_8$. Herein, ECL may be promoted at negative potentials (-1.7 V), according to the "reductive-oxidation" coreactant mechanism, where NPGs display a much higher stability. Furthermore, the signal intensity increased with the NPG porosity, as shown in Fig.12 where a fairly linear dependence of the integrated ECL intensity on the roughness factor was observed.

[Please insert here Figure 12]

These results seem to indicate that the whole surface (and volume) of the porous 3D structure, composed of interconnected wires and channels, contribute to generate the ECL signal. Intuitive detrimental phenomena like increased resistivity or diffusion hindrance in the pores would play conversely a negligible role [125].

Optically transparent electrodes (OTEs) is another vast category of electrodes which is used in ECL systems. The similarity between ITOs and Au electrodes is the extremely low porosity. On the other hand, ITO is a popular material category in sensor development due to their high conductivity and optical transmittance, wide electrochemical working window, as well as their feasibility in patterning or surface modification [126][127]. ITOs utilized in electrochemical sensors are generally modified with catalytically active metals or enzymes [128–131].

Additional catalytic abilities owing to their nanoporous morphology were recently suggested [132].

The ECL signal can be easily increased when the porosity of the material increases. Specific modifications based on spin coated ITO nanoparticles onto ITO glass substate allows to increase the porosity level as reported by Seo et al.[133]. Alternatively, ITO electrodes can be used as a layer for the deposition of nanoparticles. The result of this combination if the creation of bipolar electrodes (BPE) and the use in the ECL field. The BPEs were tested including two, three and four times spin coated ITO nanoparticles onto ITO surface, using a pristine ITO electrode to compare the ECL signal enhancement. The electrocatalytic properties of nanoporous ITO electrodes towards 5mM H_2O_2 reduction were monitored by cyclic voltammetry and electrochemical impedance spectroscopy. The cathodic current increases notably for the nanoporous ITO electrodes in comparison with the bare ITO electrode, and the onset shifted towards positive potentials. In the analysis the same types of electrodes with different porous layer thickness were compared. The ECL images of 5mM H_2O_2 are presented in Fig.13 (a) where an increasing signal was obtained upon the consecutive deposition of nanoporous ITO layers.

[Please insert here Figure 13]

This behavior indicates that BPEs implemented with nanoporous ITO layers can be operated under milder external voltages than that required for the bare ITO BPEs. This feature was further exemplified in Fig.13 (b) reporting the ECL signal of various BPEs towards 5mM H_2O_2 measured as a function of the driving potential. Nanoporous structured electrodes can also entrap reactant molecules because of their high porosity, leading to the increased interaction of the reactant with the electrode surface, resulting in enhanced catalytic effects. This catalytic mechanism based on the nanoporous morphologies has been suggested and marked as the ''nanoconfinement effect'' [134]. The thickness of these electrodes has an important effect in the ECL signal. This enhancement comes from the catalytic properties of the surface and means that the reduction of H_2O_2 is increased in the cathodic pole of the electrode. The thickness values are presented around 10-100 nm with an important limitation of nanoconfinement effect where the faradaic currents are impossible to be measured. To summarize, the entrapment of ECL reactants in the porous-based materials is an important strategy for ECL signal enhancement. Silica nanochannel-assisted electrode has been presented by Xiao et al. providing the influence of uniform pore size (2-3nm) [135]. The silica nanochannels are used as scaffold for the transaction of electrochemical reactions and by the use of this strategy can be obtained 24.8 times higher ECL signal.

CONCLUSIONS

To conclude, ECL is a powerful analytical technique that is used in different types of sensors and biosensors. The nanomaterials have a pivotal role for ECL application and a strong impact on the kinetics of electrochemical heterogeneous reactions and, therefore on the final enhancement factor of ECL analytical signal. We showed how different strategies and nanomaterial could bring into an enhance of the ECL signal compared with bare electrode.

Here we reported different class of nanomaterials such as nanoparticles-based, carbon-based hybrid materials, nanocomposite and nanoporous. The different types of nanostructured electrodes are presented for increase (i) the electrochemical potential window, (ii) the stability, (iii) new functional surfaces and (iv) open new properties to the working electrode with the final scope of enhance the efficiency of the ECL signal generation.

ACKNOWLEDGMENTS

REFERENCES

[1]   M.M. Richter, Electrochemiluminescence (ECL), (2004).

[2]   A.J.. Bard, ed., Electrogenerated Chemiluminescence, Marcel Dekker, New York, 2004.

[3]   W. Miao, ChemInform Abstract: Electrogenerated Chemiluminescence and Its Biorelated Applications, ChemInform. 39 (2008) 2506–2553. https://doi.org/10.1002/chin.200841260.

[4]   L. Hu, G. Xu, Applications and trends in electrochemiluminescence, Chem. Soc. Rev. 39 (2010) 3275–3304. https://doi.org/10.1039/b923679c.

[5]   M. Hesari, Z. Ding, Review-Electrogenerated Chemiluminescence: Light Years Ahead, J. Electrochem. Soc. 163 (2016) H3116–H3131. https://doi.org/10.1149/2.0161604jes.

[6]   N. Sojic, Analytical Electrogenerated Chemiluminescence: From Fundamentals to Bioassays., Royal Society of Chemistry, 2019.

[7]   R.T. Dufford, D. Nightingale, L.W. Gaddum, LUMINESCENCE OF GRIGNARD COMPOUNDS IN ELECTRIC AND MAGNETIC FIELDS, AND RELATED ELECTRICAL PHENOMENA, J. Am. Chem. Soc. 49 (1927) 1858–1864.

[8]   T. Mikysek, P. Nikolaou, M. Kafexholli, P. Šimůnek, J. Váňa, A. Marková, M. Vala, G. Valenti, Photophysical and Electrochemiluminescence of Coumarin-Based Oxazaborines, ChemElectroChem. 7 (2020) 1663–1676. https://doi.org/10.1002/celc.201902102.

[9]   Z. Liu, W. Qi, G. Xu, Recent advances in electrochemiluminescence, Chem. Soc. Rev. 44 (2015) 3117–3142. https://doi.org/10.1039/C5CS00086F.

[10]   A. Fiorani, G. Valenti, M. Iurlo, M. Marcaccio, F. Paolucci, Electrogenerated chemiluminescence: A molecular electrochemistry point of view, Curr. Opin. Electrochem. 8 (2018) 31–38. https://doi.org/10.1016/j.coelec.2017.12.005.

[11]   L. Chen, D.J. Hayne, E.H. Doeven, J. Agugiaro, D.J.D. Wilson, L.C. Henderson, T.U. Connell, Y.H. Nai, R. Alexander, S. Carrara, C.F. Hogan, P.S. Donnelly, P.S. Francis, Electrochemiluminescence platform for the detection of C-reactive proteins: application of recombinant antibody technology to cardiac biomarker detection, Chem. Sci. 10 (2019) 8654–8667. https://doi.org/10.1039/c9sc01391a.

[12] E.J.O. Reilly, P.J. Conroy, S. Hearty, T.E. Keyes, R.O. Kennedy, J. Forster, L. Dennany, Electrochemiluminescence platform for the detection of C-reactive proteins : application of recombinant antibody technology to cardiac biomarker detection, RSC Adv. 5 (2015) 67874–67877. https://doi.org/10.1039/c5ra08450d.

[13] W. Miao, J.P. Choi, A.J. Bard, Electrogenerated chemiluminescence 69: The Tris(2,2'-bipyridine)ruthenium(II), (Ru(bpy)32+)/tri-n-propylamine (TPrA) system revisited - A new route involving TPrA.+ cation radicals, J. Am. Chem. Soc. 124 (2002) 14478–14485. https://doi.org/10.1021/ja027532v.

[14] I. Svir, A. Oleinick, O. V. Klymenko, C. Amatore, Strong and Unexpected Effects of Diffusion Rates on the Generation of Electrochemiluminescence by Amine/Transition-Metal(II) Systems, ChemElectroChem. 2 (2015) 811–818. https://doi.org/10.1002/celc.201402460.

[15] A. Zanut, A. Fiorani, T. Saito, N. Ziebart, S. Rapino, S. Rebeccani, A. Barbon, T. Irie, H. Josel, F. Negri, M. Marcaccio, M. Windfuhr, K. Imai, G. Valenti, F. Paolucci, Insights into the mechanism of coreactant electrochemiluminescence facilitating enhanced bioanalytical performance, Nat. Commun. 11 (2020) 2668–2676. https://doi.org/10.1038/s41467-020-16476-2.

[16] M. Holzinger, A. Le Goff, S. Cosnier, Nanomaterials for biosensing applications: A review, Front. Chem. 2 (2014) 1–10. https://doi.org/10.3389/fchem.2014.00063.

[17] G. Samourgkanidis, P. Nikolaou, A. Gkovosdis-Louvaris, E. Sakellis, I.M. Blana, E. Topoglidis, Hemin-modified SnO2/metglas electrodes for the simultaneous electrochemical and magnetoelastic sensing of H2O2, Coatings. 8 (2018) 284. https://doi.org/10.3390/coatings8080284.

[18] M. Wilchek, E.A. Bayer, The avidin-biotin complex in bioanalytical applications, J. Clin. Chem. Clin. Biochem. 171 (1988) 1–32. https://doi.org/doi: 10.1016/0003-2697(88)90120-0.

[19] Meral Yuce and Hasan Kurt, How to make nanobiosensors: surface modification and characterisation of nanomaterials for biosensing applications, RSC Adv. 7 (2017) 49386–49403. https://doi.org/10.1039/c7ra10479k.

[20] P. Bertoncello, P. Ugo, Recent Advances in Electrochemiluminescence with Quantum Dots and Arrays of Nanoelectrodes, ChemElectroChem. 4 (2017) 1663–1676. https://doi.org/10.1002/celc.201700201.

[21] V. Vamvakaki, N.A. Chaniotakis, Carbon nanostructures as transducers in biosensors, Sensors Actuators, B Chem. 126 (2007) 193–197. https://doi.org/10.1016/j.snb.2006.11.042.

[22] A. Fiorani, J.P. Merino, A. Zanut, A. Criado, G. Valenti, M. Prato, F. Paolucci, Advanced carbon nanomaterials forelectrochemiluminescent biosensor applications, Curr. Opin. Electrochem. 16 (2019) 66–74. https://doi.org/10.1016/j.coelec.2019.04.018.

[23] J. Xu, Y. Zhang, L. Li, Q. Kong, L. Zhang, S. Ge, J. Yu, Colorimetric and Electrochemiluminescence Dual-Mode Sensing of Lead Ion Based on Integrated Lab-on-Paper Device, ACS Appl. Mater. Interfaces. 10 (2018) 3431–3440. https://doi.org/10.1021/acsami.7b18542.

[24] J.-T. Cao, J.-J. Yang, L.-Z. Zhao, Y.-L. Wang, H. Wang, Y.-M. Liu, S.-H. Ma, Graphene oxide@gold nanorods-based multiple-assistedelectrochemiluminescence signal amplification strategy for sensitivedetection of prostate specific antigen, Biosens. Bioelectron. 99 (2018) 92–98. https://doi.org/10.1016/j.bios.2017.07.050.

[25] S. Mehdi, H. Bagheri, M.A. Mehrgardi, Visual electrochemiluminescence biosensing of

aflatoxin M1 based onluminol-functionalized, silver nanoparticle-decorated graphene oxide, Biosens. Bioelectron. 100 (2018) 382–388. https://doi.org/10.1016/j.bios.2017.09.035.

[26] A. Zanut, A. Fiorani, S. Rebeccani, S. Kesarkar, G. Valenti, Electrochemiluminescence as emerging microscopy techniques, Anal. Bioanal. Chem. 411 (2019) 4375–4382. https://doi.org/10.1007/s00216-019-01761-x.

[27] Y. Chen, S. Zhou, L. Li, J. jie Zhu, Nanomaterials-based sensitive electrochemiluminescence biosensing, Nano Today. 12 (2017) 98–115. https://doi.org/10.1016/j.nantod.2016.12.013.

[28] Q. Zhai, J. Li, E. Wang, Recent Advances Based on Nanomaterials as Electrochemiluminescence Probes for the Fabrication of Sensors, ChemElectroChem. 4 (2017) 1639–1650. https://doi.org/10.1002/celc.201600898.

[29] E. Topoglidis, C.J. Campbell, A.E.G. Cass, J.R. Durrant, Factors that affect protein adsorption on nanostructured titania films. A novel spectroelectrochemical application to sensing, Langmuir. 17 (2001) 7899–7906. https://doi.org/10.1021/la010309b.

[30] R. Ren, Y. Zhang, B.P. Nadappuram, B. Akpinar, D. Klenerman, A.P. Ivanov, J.B. Edel, Y. Korchev, Nanopore extended field-effect transistor for selective single-molecule biosensing, Nat. Commun. 8 (2017). https://doi.org/10.1038/s41467-017-00549-w.

[31] R. Cui, L. Mei, G. Han, J. Chen, G. Zhang, Y. Quan, N. Gu, L. Zhang, Y. Fang, B. Qian, X. Jiang, Z. Han, Facile synthesis of nanoporous Pt-Y alloy with enhanced electrocatalytic activity and durability, Sci. Rep. 7 (2017) 1–10. https://doi.org/10.1038/srep41826.

[32] X. Lv, H. Ma, D. Wu, T. Yan, L. Ji, Y. Liu, X. Pang, B. Du, Q. Wei, Novel gold nanocluster electrochemiluminescence immunosensors based on nanoporous NiGd-Ni2O3-Gd2O3 alloys, Biosens. Bioelectron. 75 (2015) 142–147. https://doi.org/10.1016/j.bios.2015.08.038.

[33] G. Valenti, E. Rampazzo, S. Bonacchi, L. Petrizza, M. Marcaccio, M. Montalti, L. Prodi, F. Paolucci, Variable Doping Induces Mechanism Swapping in Electrogenerated Chemiluminescence of Ru(bpy)3 2+ Core–Shell Silica Nanoparticles, J. Am. Chem. Soc. 138 (2016) 15935–15942. https://doi.org/10.1021/jacs.6b08239.

[34] S. Kesarkar, S. Valente, A. Zanut, F. Palomba, A. Fiorani, M. Marcaccio, E. Rampazzo, G. Valenti, F. Paolucci, L. Prodi, Neutral Dye-Doped Silica Nanoparticles for Electrogenerated Chemiluminescence Signal Ampli fi cation, J. Phys. Chem. C. 123 (2019) 5686–5691. https://doi.org/10.1021/acs.jpcc.8b11049.

[35] G. Yang, Y. Yang, Y. Wang, L. Yu, D. Zhou, J. Jia, Controlled electrochemical behavior of indium tin oxide electrode modified with Pd nanoparticles via electrospinning followed by calcination toward nitrite ions, Electrochim. Acta. 78 (2012) 200–204. https://doi.org/10.1016/j.electacta.2012.05.149.

[36] J.L. Liu, Z.L. Tang, Y. Zhuo, Y.Q. Chai, R. Yuan, Ternary Electrochemiluminescence System Based on Rubrene Microrods as Luminophore and Pt Nanomaterials as Coreaction Accelerator for Ultrasensitive Detection of MicroRNA from Cancer Cells, Anal. Chem. 89 (2017) 9108–9115. https://doi.org/10.1021/acs.analchem.7b01812.

[37] Y. Qiao, Y. Li, W. Fu, Z. Guo, X. Zheng, Enhancing the Electrochemiluminescence of Luminol by Chemically Modifying the Reaction Microenvironment, Anal. Chem. 90 (2018) 9629–9636. https://doi.org/10.1021/acs.analchem.8b02577.

[38] R. de Lima, A.B. Seabra, N. Durán, Silver nanoparticles: A brief review of cytotoxicity and genotoxicity of chemically and biogenically synthesized nanoparticles, J. Appl.

Toxicol. 32 (2012) 867–879. https://doi.org/10.1002/jat.2780.

[39] S.A. Kitte, W. Gao, Y.T. Zholudov, L. Qi, A. Nsabimana, Z. Liu, G. Xu, Stainless Steel Electrode for Sensitive Luminol Electrochemiluminescent Detection of H2O2, Glucose, and Glucose Oxidase Activity, Anal. Chem. 89 (2017) 9864–9869. https://doi.org/10.1021/acs.analchem.7b01939.

[40] J. Liu, Y. Zhuo, Y. Chai, R. Yuan, BSA stabilized tetraphenylethylene nanocrystals as aggregation-induced enhanced electrochemiluminescence emitters for ultrasensitive microRNA assay, Chem. Commun. 55 (2019) 9959–9962. https://doi.org/10.1039/c9cc04660g.

[41] L. Fu, K. Fu, X. Gao, S. Dong, B. Zhang, S. Fu, H. Hsu, G. Zou, Enhanced Near-Infrared Electrochemiluminescence from Trinary Ag–In–S to Multinary Ag–Ga–In–S Nanocrystals via Doping-in- Growth and Its Immunosensing Applications, Anal. Chem. 93 (2021) 2160–2165. https://doi.org/10.1021/acs.analchem.0c03975.

[42] Q. Fang, Z. Lin, F. Lu, Y. Chen, X. Huang, W. Gao, A sensitive electrochemiluminescence immunosensor for the detection of PSA based on CdWS nanocrystals and Agþ@UIO-66-NH2 as a novel coreaction accelerator, Electrochim. Acta. 302 (2019) 207–215. https://doi.org/10.1016/j.electacta.2019.02.027.

[43] S. Liu, X. Zhang, Y. Yu, G. Zou, A monochromatic electrochemiluminescence sensing strategy for dopamine with dual-stabilizers-capped CdSe quantum dots as emitters, Anal. Chem. 86 (2014) 2784–2788. https://doi.org/10.1021/ac500046s.

[44] G. Morselli, F. Romano, G. Valenti, F. Paolucci, P. Ceroni, Silicon Nanocrystals Functionalized with Photoactive Units for Dual- Potential Electrochemiluminescence, J. Phys. Chem. B. 125 (2021) 5708–5714. https://doi.org/10.1021/acs.jpcc.1c00261.

[45] W. Khalid, M. El Helou, T. Murböck, Z. Yue, J.M. Montenegro, K. Schubert, G. Göbel, F. Lisdat, G. Witte, W.J. Parak, Immobilization of quantum dots via conjugated self-assembled monolayers and their application as a light-controlled sensor for the detection of hydrogen peroxide, ACS Nano. 5 (2011) 9870–9876. https://doi.org/10.1021/nn2035582.

[46] X. Gao, M. Geng, Y. Li, X. Wang, H.Z. Yu, Revealing and Resolving the Restrained Enzymatic Cleavage of DNA Self-Assembled Monolayers on Gold: Electrochemical Quantitation and ESI-MS Confirmation, Anal. Chem. 89 (2017) 2464–2471. https://doi.org/10.1021/acs.analchem.6b04573.

[47] S. Yang, B. Xu, J. Zhang, X. Huang, J. Ye, C. Yu, Controllable adsorption of reduced graphene oxide onto self-assembled alkanethiol monolayers on gold electrodes: Tunable electrode dimension and potential electrochemical applications, J. Phys. Chem. C. 114 (2010) 4389–4393. https://doi.org/10.1021/jp911760b.

[48] A.A. Gambardella, S.W. Feldberg, R.W. Murray, Electron transfer dynamics of iridium oxide nanoparticles attached to electrodes by self-assembled monolayers, J. Am. Chem. Soc. 134 (2012) 5774–5777. https://doi.org/10.1021/ja301212r.

[49] H. Imahori, T. Hasobe, H. Yamada, Y. Nishimura, I. Yamazaki, S. Fukuzumi, Concentration effects of porphyrin monolayers on the structure and photoelectrochemical properties of mixed self-assembled monolayers of porphyrin and alkanethiol on gold electrodes, Langmuir. 17 (2001) 4925–4931. https://doi.org/10.1021/la010006h.

[50] E.A. Speets, B.J. Ravoo, F.J.G. Roesthuis, F. Vroegindeweij, D.H.A. Blank, D.N. Reinhoudt, Fabrication of arrays of gold islands on self-assembled monolayers using pulsed laser deposition through nanosieves, Nano Lett. 4 (2004) 841–844.

https://doi.org/10.1021/nl049774u.

[51] K.Y. Hou, L. Yu, M.W. Severson, X. Zeng, Adsorption of 1,10-phenanthroline within a dodecanethiol monolayer: An approach to a switchable electrode surface, J. Phys. Chem. B. 109 (2005) 9527–9531. https://doi.org/10.1021/jp044948h.

[52] D. Samanta, A. Sarkar, Immobilization of bio-macromolecules on self-assembled monolayers: Methods and sensor applications, Chem. Soc. Rev. 40 (2011) 2567–2592. https://doi.org/10.1039/c0cs00056f.

[53] Y.P. Dong, T.T. Gao, Y. Zhou, J.J. Zhu, Electrogenerated chemiluminescence resonance energy transfer between luminol and CdSe@ZnS quantum dots and its sensing application in the determination of thrombin, Anal. Chem. 86 (2014) 11373–11379. https://doi.org/10.1021/ac5033319.

[54] F. Li, Y. Yu, H. Cui, D. Yang, Z. Bian, Label-free electrochemiluminescence immunosensor for cardiac troponin i using luminol functionalized gold nanoparticles as a sensing platform, Analyst. 138 (2013) 1844–1850. https://doi.org/10.1039/c3an36805j.

[55] Y. Li, R. Tian, X. Zheng, R. Huang, Amplified electrochemical detection of nucleic acid hybridization via selective preconcentration of unmodified gold nanoparticles, Anal. Chim. Acta. 934 (2016) 59–65. https://doi.org/10.1016/j.aca.2016.06.035.

[56] S.A. Kitte, C. Wang, S. Li, Y. Zholudov, L. Qi, J. Li, G. Xu, Electrogenerated chemiluminescence of tris(2,2'-bipyridine)ruthenium(II) using N-(3-aminopropyl)diethanolamine as coreactant, Anal. Bioanal. Chem. 408 (2016) 7059–7065. https://doi.org/10.1007/s00216-016-9409-z.

[57] S.E.K. Kirschbaum, A.J. Baeumner, A review of electrochemiluminescence (ECL) in and for microfluidic analytical devices, Anal. Bioanal. Chem. 407 (2017) 3911–3926. https://doi.org/10.1007/s00216-015-8557-x.

[58] K. Muzyka, Current trends in the development of the electrochemiluminescent immunosensors, Biosens. Bioelectron. 54 (2014) 393–407. https://doi.org/10.1016/j.bios.2013.11.011.

[59] Y. Zu, A.J. Bard, Electrogenerated chemiluminescence. 66. The role of direct coreactant oxidation in the ruthenium tris(2,2')bipyridyl/tripropylamine system and the effect of halide ions on the emission intensity, Anal. Chem. 72 (2000) 3223–3232. https://doi.org/10.1021/ac000199y.

[60] G. Valenti, A. Fiorani, H. Li, N. Sojic, F. Paolucci, Essential Role of Electrode Materials in Electrochemiluminescence Applications, ChemElectroChem. 3 (2016) 1990–1997. https://doi.org/10.1002/celc.201600602.

[61] M. Li, H. Gao, X. Wang, Y. Wang, H. Qi, C. Zhang, A fluorine-doped tin oxide electrode modified with gold nanoparticles for electrochemiluminescent determination of hydrogen peroxide released by living cells, Microchim. Acta. 184 (2017) 603–610. https://doi.org/10.1007/s00604-016-2051-9.

[62] S. Deng, Z. Hou, J. Lei, D. Lin, Z. Hu, F. Yan, H. Ju, Signal amplification by adsorption-induced catalytic reduction of dissolved oxygen on nitrogen-doped carbon nanotubes for electrochemiluminescent immunoassay, Chem. Commun. 47 (2011) 12107–12109. https://doi.org/10.1039/c1cc15766c.

[63] P. Dai, C. Liu, C. Xie, J. Ke, Y. He, L. Wei, L. Chen, J. Jin, TiO2 nanotubes loaded with CdS nanocrystals as enhanced emitters of electrochemiluminescence: application to an assay for prostate-specific antigen, Anal. Bioanal. Chem. 412 (2020) 1375–1384. https://doi.org/10.1007/s00216-019-02365-1.

[64] G. Valenti, M. Zangheri, S.E. Sansaloni, M. Mirasoli, A. Penicaud, A. Roda, F. Paolucci, Transparent Carbon Nanotube Network for Efficient Electrochemiluminescence Devices, Chem. - A Eur. J. 21 (2015) 12640–12645. https://doi.org/10.1002/chem.201501342.

[65] Q. Zhang, G. Xu, L. Gong, H. Dai, S. Zhang, Y. Li, Y. Lin, An enzyme-assisted electrochemiluminescent biosensor developed onorder mesoporous carbons substrate for ultrasensitive glyphosatesensing, Electrochim. Acta. 186 (2015) 624–630. https://doi.org/10.1016/j.electacta.2015.10.081.

[66] H. Dai, C. Yang, X. Ma, G. Chen, A highly sensitive and selective sensing ECL platform for naringin based on b-Cyclodextrin functionalized carbon nanohorns, Chem. Commun. 47 (2011) 11915–11917. https://doi.org/10.1039/c1cc14611d.

[67] D. Fang, B. Zeng, S. Zhang, H. Dai, Y. Lin, A self-enhanced electrochemiluminescent ratiometric zearalenone immunoassay based on the use of helical carbon nanotubes, Microchim. Acta. 187 (2020).

[68] G. Valenti, S. Scarabino, B. Goudeau, A. Lesch, M. Jović, E. Villani, M. Sentic, S. Rapino, S. Arbault, F. Paolucci, N. Sojic, Single Cell Electrochemiluminescence Imaging: From the Proof-of-Concept to Disposable Device-Based Analysis, J. Am. Chem. Soc. 139 (2017) 16830–16837. https://doi.org/10.1021/jacs.7b09260.

[69] A. Juzgado, A. Soldà, A. Ostric, A. Criado, G. Valenti, S. Rapino, G. Conti, G. Fracasso, F. Paolucci, M. Prato, Highly sensitive electrochemiluminescence detection of a prostate cancer biomarker, J. Mater. Chem. B. 5 (2017) 6681–6687. https://doi.org/10.1039/c7tb01557g.

[70] A. Fiorani, G. Valenti, N. Kamoshida, F. Paolucci, Y. Einaga, Electrogenerated Chemiluminescence by in Situ Production of Coreactant Hydrogen Peroxide in Carbonate Aqueous Solution at a Boron-Doped Diamond Electrode, J. Am. Chem. Soc. 142 (2020) 1518–1525. https://doi.org/10.1021/jacs.9b11842.

[71] A. Heras, A. Colina, J. López-Palacios, A. Kaskela, A.G. Nasibulin, V. Ruiz, E.I. Kauppinen, Flexible optically transparent single-walled carbon nanotube electrodes for UV-Vis absorption spectroelectrochemistry, Electrochem. Commun. 11 (2009) 442–445. https://doi.org/10.1016/j.elecom.2008.12.016.

[72] R.M. Goody, T.W. Wormell, Crystallite growth in graphitizing and non-graphitizing carbons, Proc. R. Soc. London. Ser. A. Math. Phys. Sci. 209 (1951) 196–218. https://doi.org/10.1098/rspa.1951.0197.

[73] P.J.F. Harris, Structure of non-graphitising carbons, Int. Mater. Rev. 42 (1997) 206–218. https://doi.org/10.1179/imr.1997.42.5.206.

[74] Y. Yi, G. Weinberg, M. Prenzel, M. Greiner, S. Becker, R. Schlögl, S. Heumann, Electrochemical corrosion of a glassy carbon electrode, Catal. Today. 295 (2017) 32–40. https://doi.org/10.1016/j.cattod.2017.07.013.

[75] R.L. McCreery, Advanced carbon electrode materials for molecular electrochemistry, Chem. Rev. 108 (2008) 2646–2687. https://doi.org/10.1021/cr068076m.

[76] H. Dai, C. Yang, Y. Tong, G. Xu, X. Ma, Y. Linab, G. Chen, Label-free electrochemiluminescent immunosensor for a-fetoprotein: performance of Nafion–carbon nanodots nanocomposite films as antibody carriers, Chem. Commun. 48 (2012) 3055–3057. https://doi.org/10.1039/c1cc16571b.

[77] Jiaojiao Luo, C. Zhou, Y. Shi, D. Xiao, The self-assembled Ru(bpy)3(PF6)2 nanoparticle on polystyrene microfibers and its application for ECL sensing, Analyst. 138 (2013) 6171–6176. https://doi.org/10.1039/c0xx00000x.

[78] X. Yue, Z. Zhu, M. Zhang, Z. Ye, Reaction-based turn-on electrochemiluminescent sensor with a ruthenium(II) complex for selective detection of extracellular hydrogen sulfide in rat brain, Anal. Chem. 87 (2015) 1839–1845. https://doi.org/10.1021/ac503875j.

[79] L. Jiang, Z. Fan, Design of advanced porous graphene materials: From graphene nanomesh to 3D architectures, Nanoscale. 6 (2014) 1922–1945. https://doi.org/10.1039/c3nr04555b.

[80] K. Chen, L. Chen, Y. Chen, H. Bai, L. Li, Three-dimensional porous graphene-based composite materials: Electrochemical synthesis and application, J. Mater. Chem. 22 (2012) 20968–20976. https://doi.org/10.1039/c2jm34816k.

[81] L. Qian, L. Lu, Fabrication of three-dimensional porous graphene-manganese dioxide composites as electrode materials for supercapacitors, Colloids Surfaces A Physicochem. Eng. Asp. 465 (2015) 32–38. https://doi.org/10.1016/j.colsurfa.2014.10.043.

[82] L. Qian, L. Lu, Three dimensional porous graphene-chitosan composites from ice-induced assembly for direct electron transfer and electrocatalysis of glucose oxidase, RSC Adv. 4 (2014) 38273–38280. https://doi.org/10.1039/c4ra07707e.

[83] Y. Xu, B. Zheng, T. Gao, Y. Meng, H. Yuan, D. Xiao, Improved Electrochemiluminescence Behavior of Glassy Carbon Electrode Through In Situ Chemical Bonding Modification, ChemElectroChem. 6 (2019) 1878–1883. https://doi.org/10.1002/celc.201801849.

[84] D.C. Grahame, The electrical double layer and the theory of electrocapillarity, Chem. Rev. 41 (1947) 441–501. https://doi.org/10.1021/cr60130a002.

[85] P. Nikolaou, A. Vassilakopoulou, D. Papadatos, E. Topoglidis, I. Koutselas, A chemical sensor for CBr4 based on quasi-2D and 3D hybrid organic-inorganic perovskites immobilized on TiO2 films, Mater. Chem. Front. 2 (2018) 730–740. https://doi.org/10.1039/c7qm00550d.

[86] L.A. Ioannidis, P. Nikolaou, A. Panagiotopoulos, A. Vassi, E. Topoglidis, Microperoxidase-11 modified mesoporous SnO2 film electrodes for the detection of antimalarial drug artemisinin, Anal. Methods. 11 (2019) 3117–3125. https://doi.org/10.1039/c9ay00764d.

[87] E. Topoglidis, B.M. Discher, C.C. Moser, P.L. Dutton, J.R. Durrant, Functionalizing Nanocrystalline Metal Oxide Electrodes with Robust Synthetic Redox Proteins, ChemBioChem. 4 (2003) 1332–1339. https://doi.org/10.1002/cbic.200300707.

[88] Y. Astuti, E. Topoglidis, J.R. Durrant, Use of microperoxidase-11 to functionalize tin dioxide electrodes for the optical and electrochemical sensing of hydrogen peroxide, Anal. Chim. Acta. 686 (2011) 126–132. https://doi.org/10.1016/j.aca.2010.11.045.

[89] J. Chen, L. Kong, X. Sun, J. Feng, Z. Chen, D. Fan, Q. Wei, Ultrasensitive photoelectrochemical immunosensor of cardiac troponin I detection based on dual inhibition effect of Ag@Cu2O core-shell submicron-particles on CdS QDs sensitized TiO2 nanosheets, Biosens. Bioelectron. 117 (2018) 340–346. https://doi.org/10.1016/j.bios.2018.05.037.

[90] X. Pang, H. Bian, W. Wang, C. Liu, M.S. Khan, Q. Wang, J. Qi, Q. Wei, B. Du, A bio-chemical application of N-GQDs and g-C3N4 QDs sensitized TiO2 nanopillars for the quantitative detection of pcDNA3-HBV, Biosens. Bioelectron. 91 (2017) 456–464. https://doi.org/10.1016/j.bios.2016.12.059.

[91] L. Yang, X. Liu, L. Li, S. Zhang, H. Zheng, Y. Tang, H. Ju, A visible light

photoelectrochemical sandwich aptasensor for adenosine triphosphate based on MgIn2S4-TiO2 nanoarray heterojunction, Biosens. Bioelectron. 142 (2019) 111487. https://doi.org/10.1016/j.bios.2019.111487.

[92] J. Shu, Z. Qiu, J. Zhuang, M. Xu, D. Tang, In Situ Generation of Electron Donor to Assist Signal Amplification on Porphyrin-Sensitized Titanium Dioxide Nanostructures for Ultrasensitive Photoelectrochemical Immunoassay, ACS Appl. Mater. Interfaces. 7 (2015) 23812–23818. https://doi.org/10.1021/acsami.5b08742.

[93] X. Liu, X. Huo, P. Liu, Y. Tang, J. Xu, X. Liu, Y. Zhou, Assembly of MoS2 nanosheet-TiO2 nanorod heterostructure as sensor scaffold for photoelectrochemical biosensing, Electrochim. Acta. 242 (2017) 327–336. https://doi.org/10.1016/j.electacta.2017.05.037.

[94] P. Da, W. Li, X. Lin, Y. Wang, J. Tang, G. Zheng, Surface plasmon resonance enhanced real-time photoelectrochemical protein sensing by gold nanoparticle-decorated TiO2 nanowires, Anal. Chem. 86 (2014) 6633–6639. https://doi.org/10.1021/ac501406x.

[95] X. Pang, H. Bian, M. Su, Y. Ren, J. Qi, H. Ma, D. Wu, L. Hu, B. Du, Q. Wei, Photoelectrochemical Cytosensing of RAW264.7 Macrophage Cells Based on a TiO2 Nanoneedls@MoO3 Array, Anal. Chem. 89 (2017) 7950–7957. https://doi.org/10.1021/acs.analchem.7b01038.

[96] R. Zhang, X. Zhong, A.Y. Chen, J.L. Liu, S.K. Li, Y.Q. Chai, Y. Zhuo, R. Yuan, Novel Ru(bpy) 2 (cpaphen) 2+ /TPrA/TiO 2 Ternary ECL System: An Efficient Platform for the Detection of Glutathione with Mn 2+ as Substitute Target, Anal. Chem. 91 (2019) 3681–3686. https://doi.org/10.1021/acs.analchem.8b05795.

[97] Y. Zhou, H. Wang, Y. Zhuo, Y. Chai, R. Yuan, Highly Efficient Electrochemiluminescent Silver Nanoclusters/Titanium Oxide Nanomaterials as a Signal Probe for Ferrocene-Driven Light Switch Bioanalysis, Anal. Chem. 89 (2017) 3732–3738. https://doi.org/10.1021/acs.analchem.7b00090.

[98] Y. Tang, X. Liu, H. Zheng, L. Yang, L. Li, S. Zhang, Y. Zhou, S. Alwarappan, A photoelectrochemical aptasensor for aflatoxin B1 detection based on an energy transfer strategy between Ce-TiO 2 @MoSe 2 and Au nanoparticles, Nanoscale. 11 (2019) 9115–9124. https://doi.org/10.1039/c9nr01960j.

[99] N. Liu, S. Chen, Y. Li, H. Dai, Y. Lin, Self-enhanced photocathodic matrix based on poly-dopamine sensitized TiO2 mesocrystals for mycotoxin detection assisted by a dual amplificatory nanotag, New J. Chem. 41 (2017) 3380–3386. https://doi.org/10.1039/c6nj03157a.

[100] H. Dai, G. Xu, S. Zhang, Z. Hong, Y. Lin, A ratiometric biosensor for metallothionein based on a dual heterogeneous electro-chemiluminescent response from a TiO2 mesocrystalline interface, Chem. Commun. 51 (2015) 7697–7700. https://doi.org/10.1039/c5cc01402f.

[101] E. Topoglidis, Y. Astuti, F. Duriaux, M. Grätzel, J.R. Durrant, Direct electrochemistry and nitric oxide interaction of heme proteins adsorbed on nanocrystalline tin oxide electrodes, Langmuir. 19 (2003) 6894–6900. https://doi.org/10.1021/la034466h.

[102] Y.M. Lei, R.X. Wen, J. Zhou, Y.Q. Chai, R. Yuan, Y. Zhuo, Silver Ions as Novel Coreaction Accelerator for Remarkably Enhanced Electrochemiluminescence in a PTCA-S2O82-System and Its Application in an Ultrasensitive Assay for Mercury Ions, Anal. Chem. 90 (2018) 6851–6858. https://doi.org/10.1021/acs.analchem.8b01018.

[103] S.S. Yang, M.H. Jiang, Y.Q. Chai, R. Yuan, Y. Zhuo, Application of Antibody-Powered Triplex-DNA Nanomachine to Electrochemiluminescence Biosensor for the Detection

of Anti-Digoxigenin with Improved Sensitivity Versus Cycling Strand Displacement Reaction, ACS Appl. Mater. Interfaces. 10 (2018) 38648–38655. https://doi.org/10.1021/acsami.8b16157.

[104] J.L. Liu, M. Zhao, Y. Zhuo, Y.Q. Chai, R. Yuan, Highly Efficient Intramolecular Electrochemiluminescence Energy Transfer for Ultrasensitive Bioanalysis of Aflatoxin M1, Chem. - A Eur. J. 23 (2017) 1853–1859. https://doi.org/10.1002/chem.201604411.

[105] Z. Yu, X. Wei, J. Yan, Y. Tu, Intensification of electrochemiluminescence of luminol on TiO2 supported Au atomic cluster nano-hybrid modified electrode, Analyst. 137 (2012) 1922–1929. https://doi.org/10.1039/c2an16268g.

[106] Z. Han, J. Shu, X. Liang, H. Cui, Label-Free Ratiometric Electrochemiluminescence Aptasensor Based on Nanographene Oxide Wrapped Titanium Dioxide Nanoparticles with Potential-Resolved Electrochemiluminescence, Anal. Chem. 91 (2019) 12260–12267. https://doi.org/10.1021/acs.analchem.9b02318.

[107] P.P. Dai, T. Yu, H.W. Shi, J.J. Xu, H.Y. Chen, General Strategy for Enhancing Electrochemiluminescence of Semiconductor Nanocrystals by Hydrogen Peroxide and Potassium Persulfate as Dual Coreactants, Anal. Chem. 87 (2015) 12372–12379. https://doi.org/10.1021/acs.analchem.5b03890.

[108] J. Shu, Z. Han, T. Zheng, D. Du, G. Zou, H. Cui, Potential-Resolved Multicolor Electrochemiluminescence of N-(4-Aminobutyl)-N-ethylisoluminol/tetra(4-carboxyphenyl)porphyrin/TiO2 Nanoluminophores, Anal. Chem. 89 (2017) 12636–12640. https://doi.org/10.1021/acs.analchem.7b04175.

[109] T. Wang, S. Chen, H. Pang, H. Xue, Y. Yu, MoS2-Based Nanocomposites for Electrochemical Energy Storage, Adv. Sci. 4 (2017). https://doi.org/10.1002/advs.201600289.

[110] X. Zhou, W. Zhang, Z. Wang, J. Han, G. Xie, S. Chen, Ultrasensitive aptasensing of insulin based on hollow porous C3N4/S2O82–/AuPtAg ECL ternary system and DNA walker amplification, Biosens. Bioelectron. 148 (2020) 111795. https://doi.org/10.1016/j.bios.2019.111795.

[111] Z. Yan, F. Wang, P. Deng, Y. Wang, K. Cai, Y. Chen, Z. Wang, Y. Liu, Sensitive electrogenerated chemiluminescence biosensors for protein kinase activity analysis based on bimetallic catalysis signal amplification and recognition of Au and Pt loaded metal-organic frameworks nanocomposites, Biosens. Bioelectron. 109 (2018) 132–138. https://doi.org/10.1016/j.bios.2018.03.004.

[112] Y. Li, P. Yang, P. Wang, L. Wang, Development of a novel luminol chemiluminescent method catalyzed by gold nanoparticles for determination of estrogens, Anal. Bioanal. Chem. 387 (2007) 585–592. https://doi.org/10.1007/s00216-006-0925-0.

[113] H. Wei, E. Wang, Nanomaterials with enzyme-like characteristics (nanozymes): Next-generation artificial enzymes, Chem. Soc. Rev. 42 (2013) 6060–6093. https://doi.org/10.1039/c3cs35486e.

[114] N. Hanikel, M.S. Prevot, F. Fathieh, E.A. Kapustin, H. Lyu, H. Wang, N.J. Diercks, T.G. Glover, M.O. Yaghi, Rapid Cycling and Exceptional Yield in a Metal-Organic Framework Water Harvesteŕ, ACS Sent. Sci. 5 (2019) 1699–1706. https://doi.org/10.1021/acscentsci.9b00745.

[115] L. Zhou, J. Huang, B. Yu, T. You, A novel self-enhanced electrochemiluminescence immunosensor based on hollow Ru-SiO2@PEI nanoparticles for NSE analysis, Sci. Rep. (2016) 22234. https://doi.org/10.1038/srep22234.

[116] C. Cheng, Y. Huang, X. Tian, B. Zheng, Y. Li, H. Yuan, D. Xiao, S. Xie, M.M.F. Choi, Electrogenerated chemiluminescence behavior of graphite-like carbon nitride and its application in selective sensing Cu 2+, Anal. Chem. 84 (2012) 4754–4759. https://doi.org/10.1021/ac300205w.

[117] L. Hu, J. Zheng, K. Zhao, A. Deng, J. Li, An ultrasensitive electrochemiluminescent immunosensor based on graphene oxide coupled graphite-like carbon nitride and multiwalled carbon nanotubes-gold for the detection of diclofenac, Biosens. Bioelectron. 101 (2018) 260–267. https://doi.org/10.1016/j.bios.2017.10.043.

[118] Y. Peng, Y. Li, L. Li, J.J. Zhu, A label-free aptasensor for ultrasensitive Pb2+ detection based on electrochemiluminescence resonance energy transfer between carbon nitride nanofibers and Ru(phen)32+, J. Hazard. Mater. 359 (2018) 121–128. https://doi.org/10.1016/j.jhazmat.2018.07.033.

[119] R. Li, K. Sieradzki, Ductile-brittle transition in random porous Au, Phys. Rev. Lett. 68 (1992) 1168–1171. https://doi.org/10.1103/PhysRevLett.68.1168.

[120] J. Erlebacher, M.J. Aziz, A. Karma, N. Dimitrov, K. Sieradzki, Evolution of nanoporosity in dealloying, Nature. 410 (2001) 450–453. https://doi.org/10.1038/35068529.

[121] Y. Ding, J. Erlebacher, Nanoporous metals with controlled multimodal pore size distribution, J. Am. Chem. Soc. 125 (2003) 7772–7773. https://doi.org/10.1021/ja035318g.

[122] M.C. Dixon, T.A. Daniel, M. Hieda, D.M. Smilgies, M.H.W. Chan, D.L. Allara, Preparation, structure, and optical properties of nanoporous gold thin films, Langmuir. 23 (2007) 2414–2422. https://doi.org/10.1021/la062313z.

[123] G. Ruffato, F. Romanato, D. Garoli, S. Cattarin, Nanoporous gold plasmonic structures for sensing applications, Opt. Express. 19 (2011) 13164. https://doi.org/10.1364/oe.19.013164.

[124] D. Garoli, E. Calandrini, A. Bozzola, M. Ortolani, S. Cattarin, S. Barison, A. Toma, F. De Angelis, Boosting infrared energy transfer in 3D nanoporous gold antennas, Nanoscale. 9 (2017) 915–922. https://doi.org/10.1039/c6nr08231a.

[125] E. Villani, G. Valenti, M. Marcaccio, L. Mattarozzi, S. Barison, D. Garoli, S. Cattarin, F. Paolucci, Coreactant electrochemiluminescence at nanoporous gold electrodes, Electrochim. Acta. 277 (2018) 168–175. https://doi.org/10.1016/j.electacta.2018.04.215.

[126] A. El Kasmi, M.C. Leopold, R. Galligan, R.T. Robertson, S.S. Saavedra, K. El Kacemi, E.F. Bowden, Adsorptive immobilization of cytochrome c on indium/tin oxide (ITO): Electrochemical evidence for electron transfer-induced conformational changes, Electrochem. Commun. 4 (2002) 177–181. https://doi.org/10.1016/S1388-2481(01)00299-5.

[127] E. Moore, D. O'Connell, P. Galvin, Surface characterisation of indium-tin oxide thin electrode films for use as a conducting substrate in DNA sensor development, Thin Solid Films. 515 (2006) 2612–2617. https://doi.org/10.1016/j.tsf.2006.03.025.

[128] J. Lin, W. Qu, S. Zhang, Disposable biosensor based on enzyme immobilized on Au-chitosan-modified indium tin oxide electrode with flow injection amperometric analysis, Anal. Biochem. 360 (2007) 288–293. https://doi.org/10.1016/j.ab.2006.10.030.

[129] H. Tian, M. Jia, M. Zhang, J. Hu, Nonenzymatic glucose sensor based on nickel ion implanted-modified indium tin oxide electrode, Electrochim. Acta. 96 (2013) 285–290. https://doi.org/10.1016/j.electacta.2013.02.096.

[130] J.I.A. Rashid, N.A. Yusof, J. Abdullah, U. Hashim, R. Hajian, The utilization of SiNWs/AuNPs-modified indium tin oxide (ITO) in fabrication of electrochemical DNA sensor, Mater. Sci. Eng. C. 45 (2014) 270–276. https://doi.org/10.1016/j.msec.2014.09.010.

[131] B. Reuillard, K.H. Ly, P. Hildebrandt, L.J.C. Jeuken, J.N. Butt, E. Reisner, High Performance Reduction of H2O2 with an Electron Transport Decaheme Cytochrome on a Porous ITO Electrode, J. Am. Chem. Soc. 139 (2017) 3324–3327. https://doi.org/10.1021/jacs.6b12437.

[132] M. Seo, J.H. Bae, D.W. Hwang, B. Kwak, J. Yun, S.Y. Lim, T.D. Chung, Catalytic Electron Transfer at Nanoporous Indium Tin Oxide Electrodes, Electrochim. Acta. 258 (2017) 90–97. https://doi.org/10.1016/j.electacta.2017.10.111.

[133] M. Seo, S.Y. Yeon, J. Yun, T.D. Chung, Nanoporous ITO implemented bipolar electrode sensor for enhanced electrochemiluminescence, Electrochim. Acta. 314 (2019) 89–95. https://doi.org/10.1016/j.electacta.2019.05.052.

[134] J.H. Han, E. Lee, S. Park, R. Chang, T.D. Chung, Effect of nanoporous structure on enhanced electrochemical reaction, J. Phys. Chem. C. 114 (2010) 9546–9553. https://doi.org/10.1021/jp909382b.

[135] Y. Xiao, L. Xu, P. Li, X. Tang, L. Qi, A simple microdroplet chip consisting of silica nanochannel-assisted electrode and paper cover for highly sensitive electrochemiluminescent detection of drugs in human serum, Anal. Chim. Acta. 983 (2017) 96–102. https://doi.org/10.1016/j.aca.2017.06.014.

[136] K. Imai, G. Valenti, E. Villani, S. Rapino, E. Rampazzo, M. Marcaccio, L. Prodi, F. Paolucci, Numerical Simulation of Doped Silica Nanoparticle Electrochemiluminescence, J. Phys. Chem. C. 119 (2015) 26111–26118. https://doi.org/10.1021/acs.jpcc.5b07107.
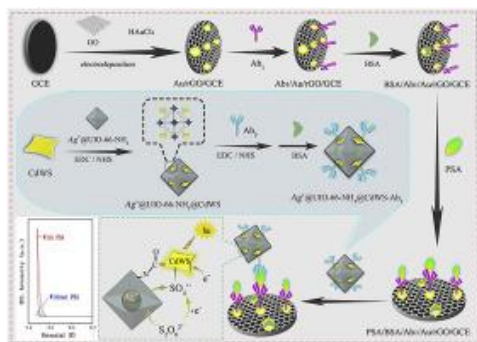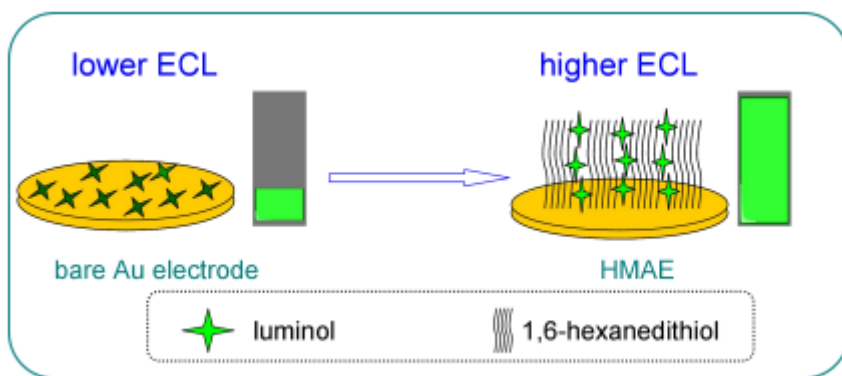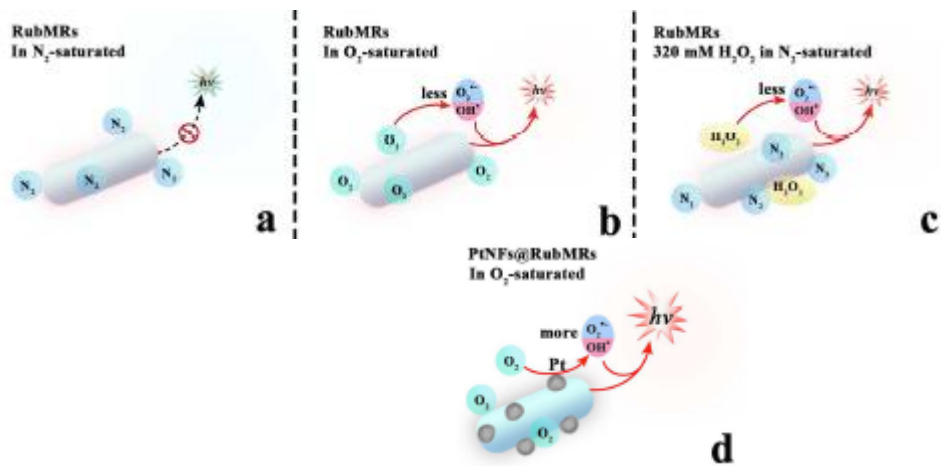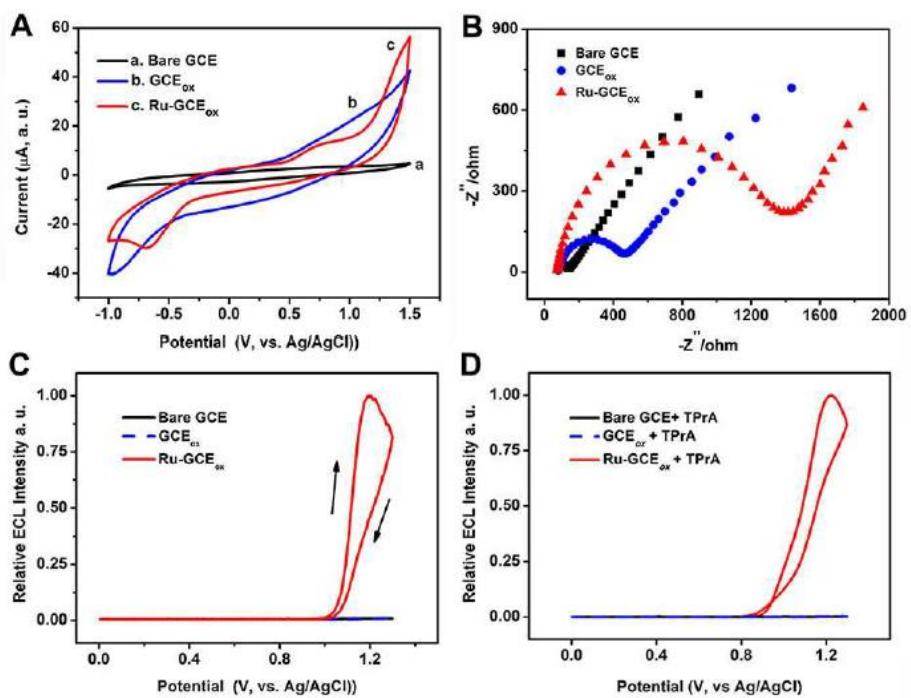
Figures
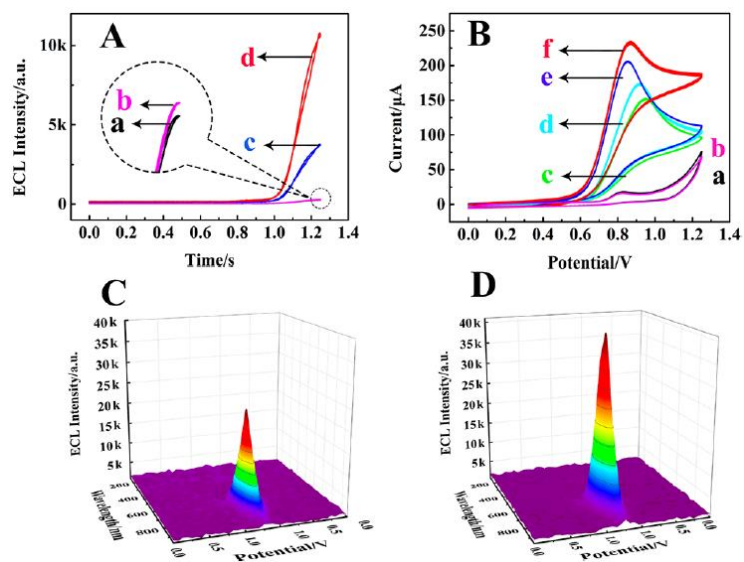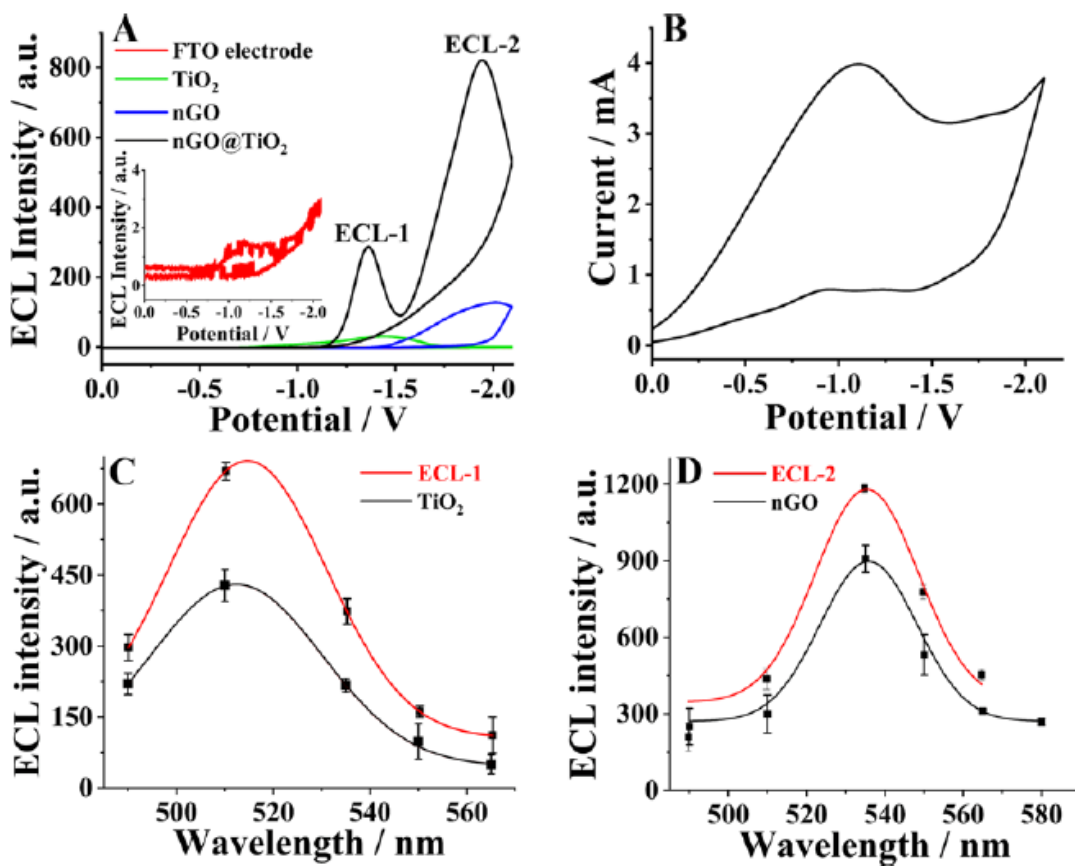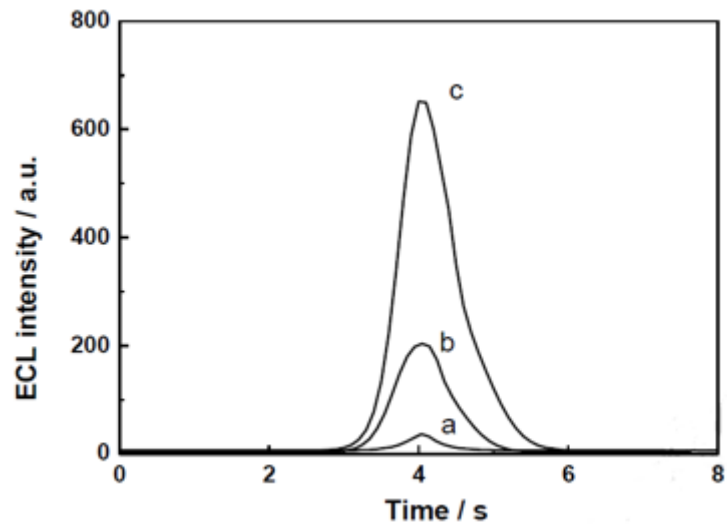
Figure 1

Figure 2

Figure 3

Figure 4

Figure 5

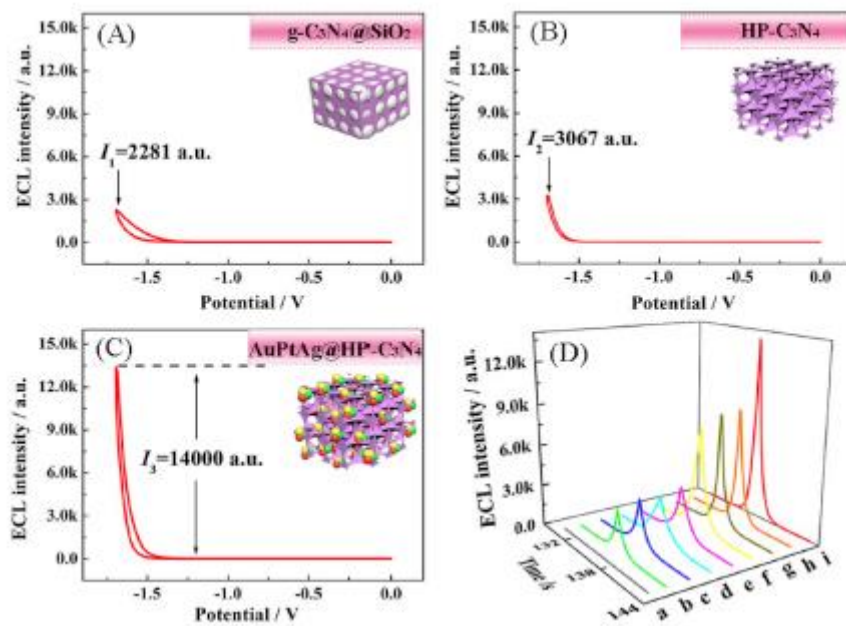Figure 6

Figure 7

Figure 8

Figure 9

Figure 10
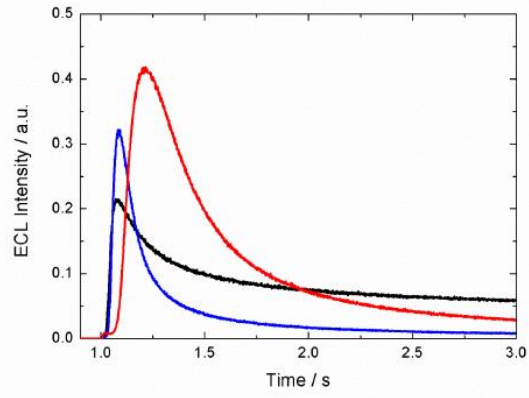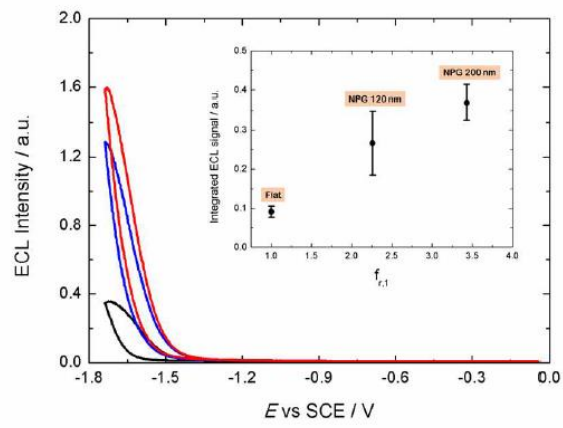
Figure 11

Figure 12
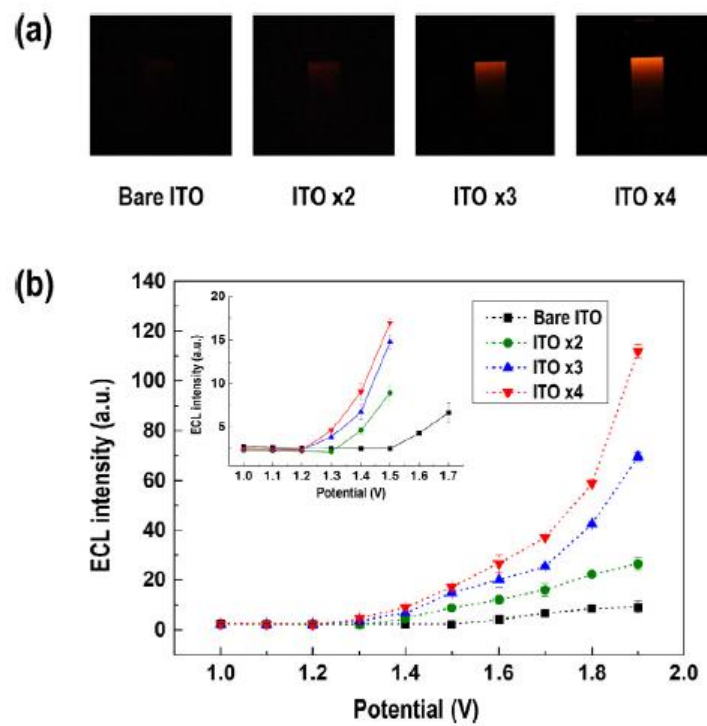
Figure 13

Caption of Figures

Caption of Figure 1: **Fig. 1**. ECL mechanisms for the couple $Ru(bpy)_3^{2+}$/TPrA: a) both luminophore and coreactant are oxidized in the "oxidative-reduction" mechanism; b) ECL generation obtained only by TPrA oxidation and involving the homogeneous reaction of the radical cation ($TPrA^{\bullet+}$), as proposed by Bard[13] .The luminophore in the excited state Ru^{2+*} relaxes to the ground state and emits photon. Reproduced from Ref. [136] , copyright 2015, with permission of American Chemical Society.

Caption of Figure 2: **Fig.2.** Top: schematic representation of a CNT-based ECL biosensor for detection of prostate cancer biomarkers Bottom: **(a)** schematic representation of the lab-on-paper device for lead ion sensing) and **(b)** scheme of the sensor assembly based on 3D nanostructured graphene aerogel for prostate-specific antigen CNT, carbon nanotube; ECL, electrochemiluminescence; rGO, reduced graphene oxide; CCD, charge coupled device; PSA, prostate specific antigen; IL, interleukin; FOND, functionalized Fe_2O_3 nano dendrites; FGA, functionalized graphene aerogel supported; TMB, 3,3',5,5'-tetramethylbenzidine; BSA, bovine serum albumin; GCE, glassy carbon electrode; NP, nanoparticles. Reproduced from Ref.[22], copyright 2019, with permission of Elsevier B.V.

Caption of Figure 3: **Fig.3.** The fabrication process of the ECL immunosensor for the detection of PSA. Reproduced from Ref.[42], copyright 2019, with permission of Elsevier B.V.

Caption of Figure 4: **Fig.4.** Activation of the luminol ECL improvement mechanism using 1,6 hexanedithiol onto Au electrode. Y. Qiao Analytical chemistry, 2018[37].
Reproduced from Ref. [37], copyright 2018, with permission of American Chemical Society.

Caption of Figure 5: **Fig.5.** The possible ECL mechanism of different electrodes: RubMRs in the N2-saturated (curve a), air-saturated (curve b), 320 mM H_2O_2 + N2-saturated (curve c), PtNFs@RubMRs/GCE in air-saturated [36]. Reproduced from Ref. [36], copyright 2017, with permission of American Chemical Society.

Caption of Figure 6: **Fig.6.** (a) CV curves of bare GCE, GCE*ox* and Ru-GCE*ox* in PBS (0.2 M, pH 7.0) without Ru-L1 under the scan rate 0.05 V/s. (b) EIS of bare GCE, GCE*ox* and Ru- GCE*ox* in 10 mM $[Fe(CN)_6]^{3+/4+}$aqueous solution. ECL signals of bare GCE, GCE*ox* and Ru-GCE*ox* in blank PBS in the absence (c) and presence (d) of TPrA at the scan rate of 0.1 V/s. Reproduced from Ref. [83], copyright 2019, with permission of Wiley-VCH Verlag GmbH & Co. KGaA, Weinheim.

Caption of Figure 7: **Fig.7.** (A) The ECL intensity of bare GCE without (a) and with (b) TiO_2 NNs in $Ru(bpy)_2(cpaphen)^{2+}$ solution, the ECL intensity of bare GCE without (c) and with (d) TiO_2 NNs in the Ru- $(bpy)_2(cpaphen)^{2+}$ + TPrA solution; (B) CVs of GCE without (a) and with (b) TiO_2 NNs in the $Ru(bpy)_2(cpaphen)^{2+}$ solution, CVs of GCE without (c) and with (d) TiO_2 NNs in the TPrA solution, CVs of bare GCE without (e) and with (f) TiO_2 NNs in the $Ru(bpy)_2(cpaphen)^{2+}$ + TPrA solution. The 3D ECL spectrum of bare GCE without (C) and with (D) TiO_2NNs/GCE in the $Ru(bpy)_2(cpaphen)^{2+}$ + TPrA solution. The concentration of $Ru(bpy)_2(cpaphen)^{2+}$ was 1.25 μM in ECL detection, ECL spectrum, and CV characterization (curve e and f); the concentration of $Ru(bpy)_2(cpaphen)^{2+}$ was 300 μM in curve a and b of CV characterization. The concentration

of TPrA in ECL detection, CV characterization, and ECL spectrum was 5 mM, 10 mM, and 5 mM, respectively [96]. Reproduced from Ref.[96]], copyright 2019, with permission of American Chemical Society.

Caption of Figure 8: **Fig.8.** (a) IECL−E curves of the FTO electrode (red line), TiO_2 (green line), nGO (blue line), and GO@TiO_2 NLPs (black line) in 0.02 mol/L PBS buffer with 0.05 mol/L $K_2S_2O_8$. The inset in part A shows enlarged IECL−E curves of the FTO electrode. (b) CV of nGO@TiO_2 NLPs. ECL spectra of (c) ECL-1 in the IECL−E curve and TiO_2. (d) ECL-2 in the IECL−E curve and nGO obtained with filters of different wavelengths. Scan rate: 0.1 V/s, scan range: 0 to −2.1 to 0 V, PMT: −500 V[106]. Reproduced from Ref.[106], copyright 2019, with permission of American Chemical Society.

Caption of Figure 9: **Fig.9.** The ECL intensity response of the phosphorylated kemptide GO/ GCE with the treatment of (a) UiO-66 probes, (b) Pt @UiO-66 probes, (c) the phosphorylated kemptide GO/ GCE with the treatment of Au&Pt @UiO-66 probes. Reproduced from Ref. [111], copyright 2018, with permission of Elsevier B.V.

Caption of Figure 10: **Fig.10.** ECL intensity-potential responses of (A) g-CeN$_4$@SiO_2/GCE (B) HP-C_3N_4/GCE and (C)AuPtAg@HP-C_3N_4/GCE, respectively. (D) ECL intensity-time response of comparison of different nanomaterials (a) to (i): bare GCE, HP-C_3N_4/GCE, Au@HP-C_3N_4/GCE, Pt@HP-C_3N_4/GCE, Ag@HP-C_3N_4/GCE, AuAg@HP-C_3N_4/GCE, AuPt@HP-C_3N_4/GCE, AgPt@HP-C_3N_4/GCE and AuPtAg@HP-C_3N_4/GCE, respectively. Reproduced from Ref. [110], copyright 2019, with permission of Elsevier B.V.

Caption of Figure 11: **Fig.11.** ECL intensity of a flat gold electrode (black line), NPG 120 nm (blue line) and NPG 200 nm (red line), analyzed in PB 200 mM, pH 6.8 with 30 mM TPrA and 0.01 mM [Ru(bpy)$_3$]Cl$_2$. Villani et al.[125]. Reproduced from Ref.[125], copyright 2018, with permission of Elsevier Ltd.

Caption of Figure 12: **Fig.12.** ECL intensity as a functional applied for flat gold electrode (black line), NPG 120 nm (blue line) and NPG 200 nm (red line). The measurements were performed in PB 200 mM, pH 6.8, with 0.01 mM [Ru(bpy)$_3$]Cl$_2$ and 50 mM (NH$_4$)$_2$S$_2$O$_8$. Scan rate: 100 mV s^{-1}. PMT bias 750 V. Inset: comparison of the integrated ECL signals obtained at the different samples reported as a function of the roughness factor Error bars show standard deviations (n=4). Villani et al. [125]. Reproduced from Ref. [125], copyright 2018, with permission of Elsevier Ltd.

Caption of Figure 13: **Fig.13.** H_2O_2 sensing system with four BPEs with different depths of ITO nanoporous layers. (a) ECL images obtained from a 5mM H_2O_2 solution under constant voltage of 1.9 V (b) ECL intensities of BPEs from 5mM H_2O_2 depending on the applied voltage, where the inset shows the enlarged view of ECL intensities at mild potentials [133]. Reproduced from Ref. [133], copyright 2019, with permission of Elsevier Ltd.